BIOCHEMICAL PHARMACOLOGY 76 (2008) 1716–1727

available at www.sciencedirect.com

ScienceDirect

journal homepage: www.elsevier.com/locate/biochempharm

Jingzhaotoxin-II, a novel tarantula toxin preferentially targets rat cardiac sodium channel

Meichi Wang, Qingping Liu, Haiyong Luo, Jiang Li, Jianzhou Tang, Yucheng Xiao, Songping Liang *

Key Laboratory of Protein Chemistry and Developmental Biology of the Ministry of Education, College of Life Science, Hunan Normal University, Changsha 410081, PR China

ARTICLE INFO

Article history:
Received 20 July 2008
Accepted 5 September 2008

Keywords:
Tetrodotoxin-sensitive
Tetrodotoxin-resistant
Dorsal root ganglion
Dorsal unpaired median
Cardiac myocytes

ABSTRACT

Naturally occurring toxins are invaluable tools for exploration of the structure and function relationships of voltage-gated sodium channels (VGSCs). In this study, we isolated and characterized a novel VGSC toxin named jingzhaotoxin-II (JZTX-II) from the tarantula *Chilobrachys jingzhao* venom. JZTX-II consists of 32 amino acid residues including two acidic and two basic residues. Cloned and sequenced using 3′- and 5′-rapid amplification of the cDNA ends, the full-length cDNA for JZTX-II was found to encode a 63-residue precursor which contained a signal peptide of 21 residues, a propeptide of 10 residues and a mature peptide of 32 residues. Under whole-cell voltage-clamp conditions, JZTX-II significantly slowed rapid inactivation of TTX-resistant (TTX-R) VGSC on cardiac myocytes with the $IC_{50} = 0.26 \pm 0.09$ μM. In addition, JZTX-II had no effect on TTX-R VGSCs on rat dorsal root ganglion neurons but exerted a concentration-dependent reduction in tetrodotoxin-sensitive (TTX-S) VGSCs accompanied by a slowing of sodium current inactivation similar to delta-ACTXs. It is notable that TTX-S VGSCs on cultured rat hippocampal neurons were resistant to JZTX-II at high dose. Based on its high selectivity for mammalian VGSC subtypes, JZTX-II might be an important ligand for discrimination of VGSC subtypes and for exploration of the distribution and modulation mechanisms of VGSCs.

1. Introduction

Voltage-gated sodium channels (VGSCs) structurally conserved in vertebrates and invertebrates, play a pivotal role in cellular excitability. The complexity of VGSC subtypes expression suggests that the particular isoforms may have specialized roles in different physiological systems [1]. They are composed of a functional pore-forming α-subunit (260) kDa and up to four auxiliary β-subunits. The α-subunit is composed of four homologous domains (D1–D4), each with six transmembrane segments (S1–S6) and a hairpin-like pore region between S5 and S6 [2]. To date, at least nine VGSC isoforms (Nav1.1–1.9) encoded by a gene family have been cloned and functionally characterized from mammalian tissues [3]. Their expression is restricted to specific tissues. For example, some are broadly expressed in the central nerve system (rNav1.1–1.3, rNav1.6), whereas others are expressed in the peripheral nervous system (rNav1.7), sensory neurons with a small diameter (rNav1.8 and rNav1.9), skeletal muscle (rNav1.4), and cardiac muscle (rNav1.5) [4]. They are classified

* *Corresponding author*. Tel.: +86 731 8872556; fax: +86 731 8861304.
E-mail address: liangsp@hunnu.edu.cn (S. Liang).

Abbreviations: JZTX-II, jingzhaotoxin-II; RACE, rapid amplification of cDNA end; TTX-S, tetrodotoxin-sensitive; TTX-R, tetrodotoxin-resistant; DRG, dorsal root ganglion; DUM, dorsal unpaired median; RP-HPLC, reverse-phase high performance liquid chromatography; MALDI-TOF, matrix-assisted laser desorption/ionization time-of-flight mass spectrometry.

0006-2952/$ – see front matter © 2008 Published by Elsevier Inc.
doi:10.1016/j.bcp.2008.09.008

into two groups, TTX-resistant (TTX-R) (rNav1.5, 1.8 and 1.9) and tetrodotoxin-sensitive (TTX-S) (rNav1.1-1.4, 1.6 and 1.7) VGSCs. Sequence analysis demonstrates that they have been highly conserved during evolution (NCBI, core nucleotide databank).

The activities of VGSCs can be modulated by a large variety of chemically distinct toxins. Although many of them do not distinguish between VGSC subtypes [5], some scorpion neurotoxins show specificity for insect or mammalian VGSCs [6]. This selectivity is attributed to the distinct distribution of active sites on animal toxins and to variations in receptor binding sites on different VGSC isoforms. During evolution, various animals have developed a set of cysteine-rich peptides capable of binding different extracellular sites of channel proteins [7]. There are at least seven neurotoxin receptor sites on mammal ion sodium channels [8]. Animal toxins have facilitated the functional mapping of sodium channels by virtue of binding to different receptor sites and selectively interacting with channel variants. Spider venom contains many neurotoxins demonstrated to target VGSCs. For example, δ-ACTXs from Australian funnel-web spiders and μ-agatoxins from *Agelenopsis aperta* bind to receptor site 3 by slowing down sodium channel inactivation [9], whereas, Css2 and Css4 from *Centruroides suffusus suffuses* and Tzl from the Venezuelan scorpion *Tityus zulianus* fail to inhibit VGSC inactivation have been shown not to bind to receptor site 3 but to site 4 [10]. ProTx-II from the venom of the tarantula, *Thrixopelma pruriens*, was found neither site 3 nor site 4 neurotoxin of VGSCs and made it a novel probe of activation gating in Nav channels [11].

Come from the venom of Chinese tarantula *Chilobrachys jingzhao*, several ion channel toxins had been isolated and characterized. JZTX-I was a neurotoxin preferentially inhibiting cardiac sodium channel inactivation [12]; JZTX-III was a novel spider toxin inhibiting activation of voltage-gated sodium channel in rat cardiac myocytes [13,14]; JZTX-V a potent Na^+ channels on DRG neurons and Kv4.2 channels inhibitor [15]; JZTX-XI had the promiscuous activity on both Kv2.1 and Nav1.5 channels [16]; JZTX-XII was a gating modifier specific for Kv4.1 channels [17]. In this study, we report the isolation, sequencing, cDNA and functional characterization of a novel toxin from the tarantula *C. jingzhao*, denoted as jingzhaotoxin-II (JZTX-II). Composed of 32 residues with six cysteines, JZTX-II shows no effects on TTX-R VGSCs from adult rat peripheral neurons and TTX-S VGSCs from cultured rat central neurons. The toxin inhibits fast inactivation of peripheral neuron TTX-S and cardiac TTX-R VGSC subtypes. Moreover, JZTX-II, like δ-ACTXs, inhibits TTX-S VGSCs in cockroach dorsal unpaired median (DUM) neurons [8,18].

2. Materials and methods

2.1. Materials and animals

Sprague–Dawley rats were purchased from Xiangya School of Medicine, Central South University. Cockroaches were from our laboratory stock colonies. All sequencing reagents were purchased from Applied Biosystems (Foster City, CA, USA), Division of Perkin-Elmer. The 3′- and 5′-RACE kits and Trizol reagent were purchased from Invitrogen Inc. (Grand island, NY, USA). Taq DNA polymerase and TFA were obtained from Sigma (St. Louis, MO, USA). DTT, Iodoacetamide, Trypsin (Proteomics Sequencing Grade) and TFA were obtained from Sigma (St. Louis, MO, USA). Acetonitrile is domestic product (chromatogram-grade). Other chemicals are domestic products (analytical-grade). The water used was de-ionized in a Milli-Q system (Millipore, Bedford, MA, USA).

2.2. Purification of JZTX-II

Venom was obtained by manual stimulation [19]. The freeze-dried crude venom was stored at −20 °C prior to analysis. Lyophilized crude venom was suspended in distilled water, centrifuged (2000 × *g*, 4 °C, 10 min) and filtered through 0.45 μm microfilter before loaded onto the column. JZTX-II was purified by a combination of ion-exchange HPLC and reverse-phase HPLC as described [12]. First, filtered venom was loaded onto a Water Protein-Pak CM anode ion-exchange column (1 cm × 10 cm). The eluting solution was composed with 9% 0.1 M NaH_2PO_4 (pH 6.0) and 1% 0.1 M Na_2HPO_4 (pH 6.0) with a linear gradient of 0–90% of buffer C (1 M NaCl, pH 6.0) at a flow rate of 1 ml/min. The solution D was distilled H_2O. The fraction of interested was then applied to an Elite C18 reverse-phase column (10 mm × 250 mm) and eluted at a flow rate of 1 ml/min using a gradient of 0–50% buffer B (0.1% TFA in acetonitrile) after equilibration with buffer A (0.1% TFA in water) for 10 min. The eluted fraction of retention time 33.14 min by Elite C18 column was lyophilized and was further purified by a Vydac C18 analytical RP-HPLC column (3.9 mm × 300 mm) by a gradient of 10–50 buffer B (as above) over 40 min at a flow rate of 0.7 ml/min. Purified toxin was collected, lyophilized and stored at −20 °C until required.

2.3. Mass spectrometry analysis and Edman sequencing

Molecular mass analysis of the toxin was performed on a Voyager-DE™ STR MALDI-TOF mass spectrometer of ABI Company. After the average molecular mass of JZTX-II was determined, the monoisotopic relative molecular mass was also chosen for analysis from the whole isotopic molecular mass. The entire amino acid sequence was obtained from a single sequencing run on an Applied Biosystems/Perkin-Elmer Life Sciences Procise 491-A protein sequencer.

cDNA amplification and sequence analysis of JZTX-II cDNA sequence of JZTX-II was obtained using the method of RACE [12,13]. Total RNA of spider *C. jingzhao* was extracted from the venom gland which was isolated and frozen in liquid nitrogen. For 3′-RACE, primer 5′-TG(C/T)GG(A/C/G/T)AC (A/C/G/T)ATGTGG (A/T) (G/C)(A/T/G/C)CC-3′ (based on the peptide sequence of ^{2}CGTMWSP^{8}) and its nested primer 5′-TG (C/T)GA(C/T)AA(C/T) TT(C/T)(A/T)(G/C)(A/T/G/C)TG(C/T)CA-3′ (based on the peptide sequence of ^{16}CDNFSCQ^{22}) were designed and synthesized for PCR amplification. The amplified 3′ fragment was then cloned into the pGEX-T easy vector for sequencing. Based on the obtained 3′ cDNA sequence, 5′-RACE primer 5′-AGGACTTCAATGGCCTAAGG-3′ (based on the 3′ untranslated sequence) and its nested primer 5′-CTAAGGGCTCCAGATGC ACC-3′ (based on the based on the 3′ untranslated sequence) were also synthesized and used

for 5′-RACE amplification. The whole cDNA sequence of JZTX-II was completed by overlapping 3′-RACE and 5′-RACE fragments.

2.4. Acute isolation of DRG neurons

All procedures were conformed to the guidelines of the National Institutes of Health Guide for the Care and Use of laboratory Animals and approved by the Animal Care and Use committee of the Hunan Normal University College of Medicine [12]. Briefly, DRG neurons were isolated from adult rat: 180–200 g adult Sprague–Dawley rats of either sex. DRG from the spinal cord were removed and transferred immediately into ice-cold DMEM (Gibco). Stripped of their connective tissue capsules, transferred into another ice-cold DMEM and then minced with scissor, DRG were transferred into 5 ml DMEM containing trypsin, collagenase to incubate at 34 °C. Trypsin inhibitor was used to terminate enzyme treatment. DMEM solution had been centrifuged at 800 r/min for 5 min. The neurons were newly suspended in the 90% DMEM, 10% newborn calf serum. Cultured neurons were kept at 37 °C in a CO_2 incubator containing 5% CO_2 and were used between 4 h and 24 h.

2.5. Acute isolation of rat ventricular cardiomyocytes

Single ventricular cardiomyocytes were enzymatically dissociated from adult rats [13,20]. Briefly, Sprague–Dawley rats 200–250 g of either sex were killed by decapitation with slight anesthetization. The heart was rapidly removed and rinsed in Tyrod's solution NaCl 143 mM, KCl 5.4 mM, $MgCl_2$ 0.5 mM, HEPES 5.0 mM, NaH_2PO_4 0.3 mM, Glucose 5.5 mM, $CaCl_2$ 1.8 mM. The heart beat rhythmically now. Then the heart was mounted on a Langendorff apparatus for retrograde perfusion via the aorta with recirculating Ca^{2+}-free Tyrode's solution bubbled by 95% O_2 and 5% CO_2 at 37 °C. After that, the perfusate was switched to a Ca^{2+}-free Tyrode's solution supplemented with Collagenase IA and BSA, and the heart was perfused in a recirculated mode for 5 min. After the enzymatic solution was replaced by Kraftbrühe (KB) solution buffer containing L-glutamic acid 70 mM, KCl 25 mM, Taurine 20 mM, KH_2PO_4 10 mM, $MgCl_2$ 3 mM, EGTA 0.5 mM, Glucose 10 mM, HEPES 10 mM at pH 7.4, the partially digested hearts were cut, minced and gently triturated. The single cells were obtained and transferred into 35 mm culture dishes. All cells were used within 8 h after separation.

2.6. Acute isolation of DUM neurons

Experiments were carried out on single dorsal unpaired median neurons acutely isolated from the adult cockroach *Periplaneta americana* [21]. The sheaths had been excised, the abdominal ganglia was exposed, then excised and incubated in insect physiological solution (in mM) containing: 90 NaCl, 6 KCl, 2 $CaCl_2$, 2 $MgCl_2$, and 10 HEPES, 140 Glucose, 1 mg/ml trypsin, pH 6.6 for 10 min. After the enzyme was thoroughly washed off and the ganglia were stored in physiologic solution for 1 h, the large DUM cells situated in the dorsal midline of the ganglia were separated with the use of thin silver needles. Viability of cells was assessed by microscopic observation: only those having a bright appearance under phase contrast were used [22].

2.7. Hippocampal neuron culture

Hippocampal neurons from embryonic rats (E18) were obtained [23]. Hippocampal tissues from 18-day-old fetal rats were dissected and treated with 0.25% trypsin in Ca^{2+}–Mg^{2+}-free Hank's Buffered Salt Solution at 37 °C for 15 min; they were then dissociated by trituration with a glass Pasteur pipette and plated in 35 mm culture dishes with glass bottoms (MatTek, Ashland, MA, USA) for culture and subsequent microscopy. The glass surface in each dish (35 mm diameter) was pretreated with poly-D-lysine for one night (500 μg/ml in borate buffer), washed three times, and air-dried before cell plating. Approximately 35,000 cells in DMEM containing 10% fetal bovine serum were plated in the glass area of each dish. On the second day after plating, the culture medium was replaced by serum-free Neurobasal medium containing 2% B27 supplement. 500 μmol/l glutamine was used to reduce the growth of glial cells. Neurons were maintained in a CO_2 incubator at 37 °C, and one-half volume of the culture medium was replaced with fresh Neurobasal medium containing 2% B27 supplement every other day. The neurons were used for electrical physiological studies after culture for 10 days.

2.8. Electrophysiological studies

Sodium current recording was performed using whole-cell patch clamp technique through an EPC-9 patch clamp amplifier (HEKA Electronics, Germany). Suction pipettes were made from borosilicate glass capillary tubes with a two-step pulling from a vertical micropipette puller (PC-10, Narishige). To record sodium currents from DRG neurons, micropipettes were filled with a solution containing (in mM): 105 CsF, 35 NaCl, 10 HEPES, and 10 EGTA (pH was adjusted to 7.4 with CsOH). The external solution contains (in mM): 50 NaCl, 100 TEA.Cl, 2 KCl, 1.5 $CaCl_2$, 10 HEPES, 1 $MgCl_2$, and 5 Glucose (pH was adjusted to 7.4 with HCl). TTX at 0.2 μM was used to inhibit TTX-S sodium currents and obtain TTX-R sodium currents. Single ventricular cardiomyocytes were selected based on clear striations. 30 mM NaCl exist in external solution for recording cardiac myocytes sodium currents. To record sodium currents from hippocampal neurons, the external solution contains (in mM): 150 NaCl, 5 KCl, 1 $MgCl_2$, 10 Glucose, 10 HEPES, pH was adjusted to 7.4. To record sodium currents from insect DUM neurons, the external solution contains (in mM): 80 NaCl, 30 TEA.Cl, 2 $CaCl_2$, 4 KCl, 10 HEPES, 10 Glucose, 50 choline-Cl, 1 4-AP (pH was adjusted to 6.8) and the micropipette internal solution contains (in mM): 140 CsF, 2 $MgCl_2$, 10 EGTA, 10 HEPES with pH 6.8. Drug containing solutions of 10 μl volume were applied by low pressure injection with a microinjector (IM-5B, Narishige, Tokyo, Japan). All experiments were completed at room temperature 22–25 °C. Experiments data were acquired and analyzed by using the program Pulse/Pulsefit 8.0 (HEKA Electronics, Germany). Leakage and capacitive currents were digitally subtracted with P/4 protocol and series resistance was kept at 3–5 MΩ and compensated 75–85% for all cells.

2.9. Data analysis

Experimental data were acquired and analyzed by the program pulse + pulsefit8.0 (HEKA, Germany). Data analysis performed using Sigmaplot. All data are presented as mean ± standard error and n is the number of independent experiments. The degree of fast inactivation was assayed by measuring the I_{5ms}/I_{peak} ratio, which gives an estimate of the probability for the channels not to be inactivated after 5 ms [24]. The steady-state Na^+ channels inactivation (I_{test}/I_{max}) were obtained by using the following form of the Boltzmann equation:

$$\frac{I_{test}}{I_{max}} = \frac{1}{[1 + \exp(V - V_{1/2})/K]}$$

where I_{test} is the peak amplitude of I_{Na} at −10 mV test pulse from a holding potential of −130 to −20 mV. V is the different prepulse potential, $V_{1/2}$ is the voltage of half inactivation and K is the slope factor.

2.10. Evolutionary tree of spider sodium channel toxins

The phylogeny of spider sodium channel toxins was constructed as described previously. In our study, we focused on the spider toxins from the species in the family *Mygalomorphae but not* the family *Araneomorphae* to outline the phylogeny clearly [12]. Multiple sequences of spider toxins were edited using the Bioedit Sequence Alignment Editor software and then aligned and refined manually using ClustalW1.8 program. A pairwise distance matrix was calculated on the basis of the proportions of different amino acids. The matrix was then used to construct trees by the neighbor-joining method (MEGA3.1). The reliability of branching patterns was assessed using 1000 bootstrap replications.

3. Results

3.1. Purification and sequence analysis of JZTX-II

The venom containing JZTX-II was purified from the crude venom from the spider *C. jingzhao* using a method combining ion-exchange HPLC on a Waters Protein-Pak CM 8H column and repeated reverse-phase HPLC on a Vydac C18 column. Fig. 1A shows a typical ion-change HPLC chromatogram of the crude spider venom and nine main fractions were eluted monitored at 280 nm. The peak labeled with an asterisk (Fig. 1A), which was eluted at 11.2 min with about 20% NaCl was further purified by RP-HPLC to yield more than 10 fractions. Among them, the peak of retention time 33.14 min marked with an asterisk, eluted with a gradient of about 40% acetonitrile (Fig. 1B) was further fractionated on an analytical RP-HPLC column (Fig. 1C). The purity of JZTX-II was over 99% assessed by RP-HPLC and N-terminal sequence analysis. The molecular mass of the naturally occurring toxin was determined to be 3561.13 Da by MALDI-TOF mass spectrometry (Fig. 1D). It was composed of 32 residues including six cysteine residues (Fig. 2A). Its full amino acid sequence was determined by Edman degradation and found to be GCGTMWSPCSTE KPCCDNFSCQPAIKWCIWSP. The predicted molecular mass of primary sequence (3567.17 Da) is 6 Da great than the spectrometer mass, implying that all six cysteine residues are involved in forming three disulfide bonds

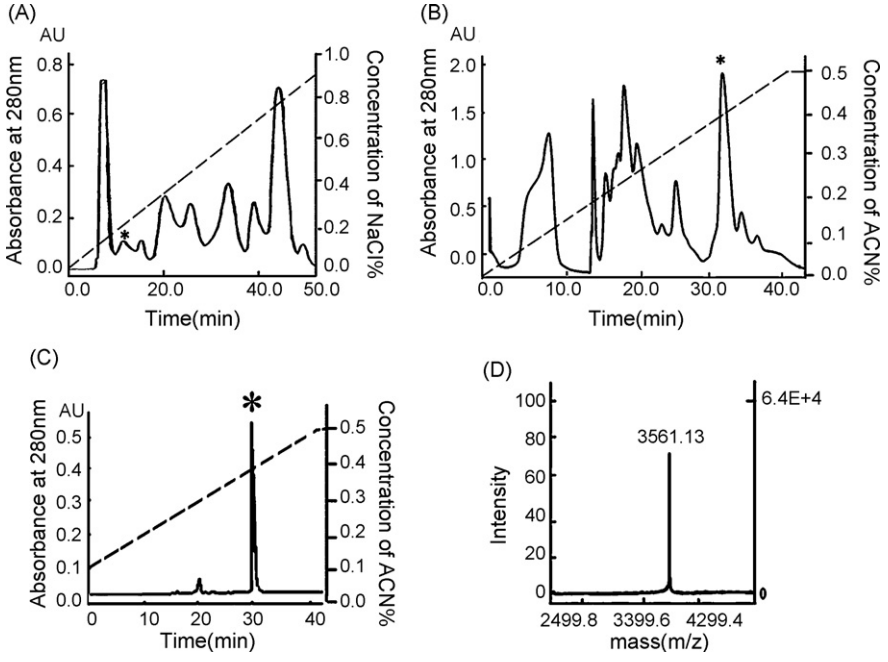

Fig. 1 – Purification and mass identification of JZTX-II. (A) Ion-exchange HPLC chromatogram of the crude venom. An asterisk indicates that the fraction with a retention time of 11.2 min contains the component of interest. (B) Reverse-phase HPLC profile of the interest fraction from the ion-exchange HPLC. An asterisk indicates that the fraction with a retention time of 32.02 min contains the JZTX-II of interest. (C) Analytical reverse-phase HPLC profile of the interest fraction from the RP-HPLC on C18 column. An asterisk indicates the goal toxin. (D) The typical MALDI-TOF mass spectrometry analysis of JZTX-II. The molecular mass of natural toxin JZTX-II is 3561.13 Da.

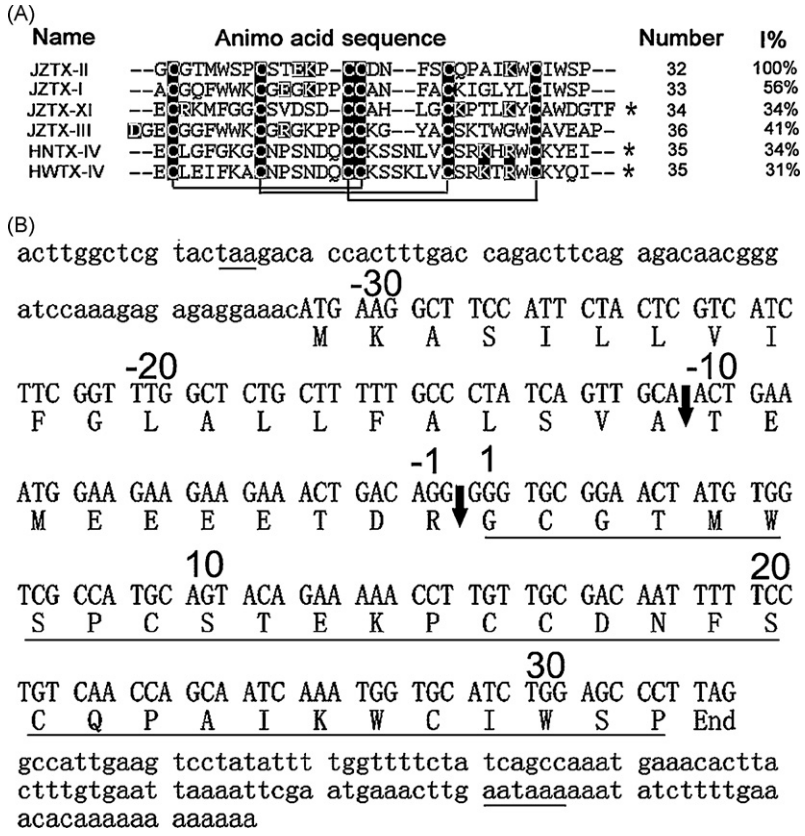

Fig. 2 – Amino acid sequence and cDNA sequence of JZTX-II. (A) The sequence alignment of JZTX-II with some other toxins. JZTX-I, JZTX-III and JZTX-XI had been isolated from *Chilobrachys jingzhao*, HNTX-IV was from *Ornithoctonus hainana* and HWTX-IV was from *Ornithoctorus huwena* (13, 23, 33). The well-conserved cysteine residues are in black. The putative crucial residues are shaded in *black*. The conserved disulfide bridge pattern of these toxins is indicated under their sequences. An asterisk indicates the amidation at the C-terminal carboxyl group. The percentage identity (%) is shown to be the right of the sequence. (B) The oligonucleotide sequence of JZTX-II cDNA. The amino acid composition of the precursor reading from the cDNA is suggested below the nucleotide sequence. The potential endoproteolytic sites are indicated with down arrows. The sequence of mature peptide is underlined by solid line.

and the C-terminal residue (Pro32) is not amidated. The amino acid residues of JZTX-II are arranged as $CX_6CX_5CX_0CX_4CX_6C$ (where X is any residue and the number shows the number of residues) this is suitable for the half-cysteine space definition for ICK motif: $CX_{3-7}CX_{4-6}CX_{0-5}CX_{0-4}$ $CX_{3-13}C$ (where X is any residue, with the number indicating the range) [25]. Further analysis shows that $CX_6CX_5CX_0CX_4CX_6C$ belongs to motif 1.1.0.1.n, the mostly prevalent toxin motif classified by Kozlov and Grishin [26]. JZTX-II is a novel tarantula toxin exhibiting limited sequence identity with any reported spider neurotoxin peptide but 50% with JZTX-I. Despite the significant sequence divergence, sequence alignment indicated that all six cysteines in JZTX-II were strictly conserved at similar positions (Fig. 2A) in other peptides which adopting a typical ICK fold such as JZTX-III and JZTX-XI [14,16]. JZTX-II might adopt the typical tertiary structure of ICK motif.

3.2. *Cloning and sequencing JZTX-II cDNA*

The full-length cDNA sequence of JZTX-II was completed by overlaying two fragments resulting from 3′- and 5′-RACE. As shown in Fig. 2B, the oligonucleotide sequence of the cDNA had 378-nt found to comprise a 5′-untranslated region (5′-UTR), an open reading frame and a 3′-untranslated region (3′-UTR). The open reading frame encoded a 63-residue peptide corresponding to the JZTX-II precursor, which contained a signal peptide of 21 residues, a propeptide of 10 residues and a mature peptide of 32 residues. The pre-pro-region composed of signal peptide and propeptide is a hydrophobic peptide common to other toxins, such as JZTX-I. Unlike most spider sodium channel toxins such as JZTX-XI, HNTX-IV and HWTX-IV [16], JZTX-II had no extra amino acid residues G or G + R/K at its C-terminus known to allow ''post-modification'' α-amidation at the C-terminal residue, implying that the C-terminal residue of the mature toxin is not amidated. A polyadenylation signal (AATAAA) emerged in the 3′-UTR at position 18 upstream of the poly (A) as usual [12].

3.3. *Effects of JZTX-II on various sodium channel subtypes*

Sodium channels expressing in different tissues have been shown to be different subtypes, based on divergent amino acid sequences. According to the basic gating kinetics and sensitivity to the puffer fish toxin, tetrodotoxin, sodium channels have

been classified into TTX-S and TTX-R types. TTX-S and TTX-R VGSCs are co-expressed on adult rat DRG neurons [27], whereas only TTX-S VGSCs are distributed in hippocampal neurons [28] and TTX-R VGSC is the primary type in adult rat ventricular myocytes on mammals [29]. Using whole-cell patch clamp technique, the actions of JZTX-II were characterized on different kinds of excitable cells. Current traces were evoked using a 50 ms or 20 ms step depolarization to −10 mV from a holding potential of −80 mV every 2 s. TTX (200 nM) was added to the external bath solution to separate TTX-R type from mixture currents. Fig. 3 shows the effect of JZTX-II on sodium currents from different tissues. The effect of the toxin was assayed by measuring the I_{5ms}/I_{peak} ratio which gave an estimate of the probability of the channel not to be inactivated after 5 ms. JZTX-II inhibited current amplitude and the inactivation of TTX-S VGSCs on rat DRG sensory neurons (Fig. 3A, $n = 5$) and cockroach DUM neurons (Fig. 3B, $n = 5$) in a dose- (Fig. 3F, $n = 5$) and time-dependent pattern (Fig. 4A, $n = 5$; Fig. 4C, $n = 5$). The IC_{50} was 0.83 ± 0.15 μM and 1.9 ± 0.07 μM, respectively (Fig. 3F). JZTX-II at 10 μM were resistant to TTX-R VGSCs on rat DRG sensory neurons (Fig. 3D, $n = 5$), while lower concentration JZTX-II are sensitive to TTX-R VGSCs on rat cardiac myocytes (Fig. 3C). JZTX-II at 1 μM inhibited inactivation of TTX-R VGSCs on rat cardiac myocytes by 85.2 ± 3.4% in a time-dependent pattern and had no significant reduction to the peak current amplitude (Fig. 3C, $n = 5$). The IC_{50} was 0.26 ± 0.09 μM (Fig. 3F). Evidently, the slowing potency of JZTX-II on sodium subtypes was much higher on rat cardiac myocytes than on rat DRG neurons. However, JZTX-II exhibited completely distinct effect on isoforms of neuronal TTX-S VGSCs. At a concentration of 10 μM, JZTX-II did not significantly change the amplitude and kinetics of TTX-S VGSCs on rat hippocampal neurons (Fig. 3E, $n = 5$).

3.4. *Effects of JZTX-II on the activation and inactivation kinetics of voltage-gated sodium channels*

Fig. 5 shows the current–voltage (I–V) curves of the TTX-S sodium channel, which give the initial activated voltage and reversal potential. The current traces were evoked using a 50 ms step depolarization from −80 mV to +50 mV under

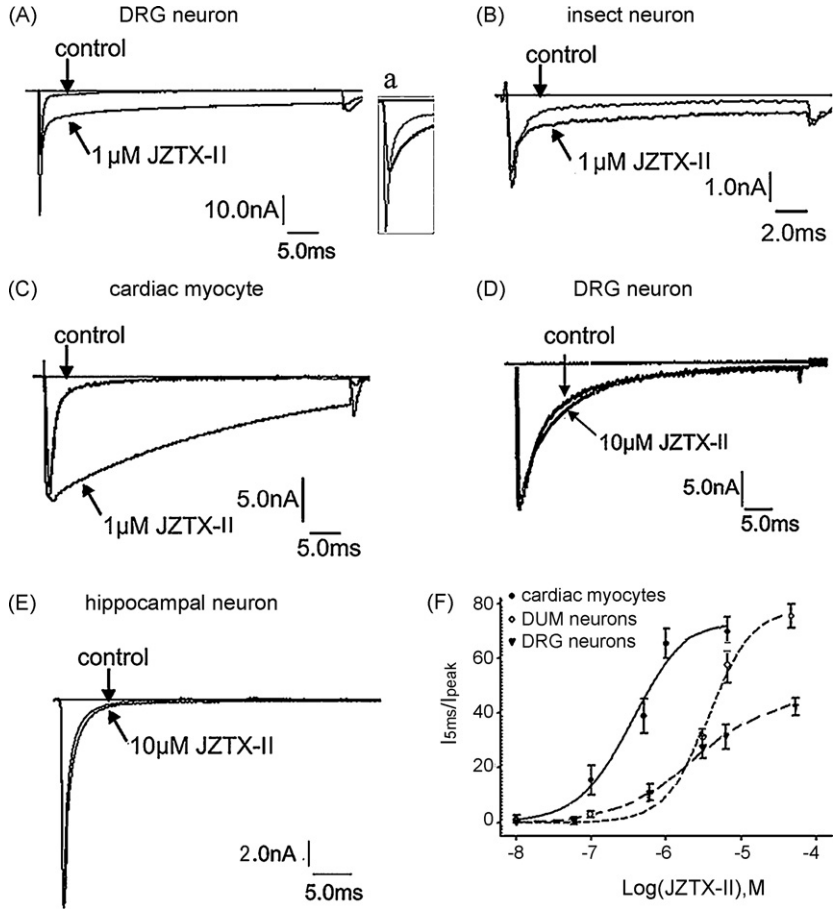

Fig. 3 – Effects of JZTX-II on TTX-S and TTX-R sodium currents. Current traces were elicited by a 50 ms or 20 ms depolarizing potential of −10 mV from a holding potential −80 mV. (A) Representative typical TTX-S sodium current traces in the absence or presence of 1 μM JZTX-II on rat DRG neurons. (B) Typical TTX-S sodium current traces on cockroach DUM neurons in the absence or presence of 1 μM JZTX-II. (C) Representative TTX-R sodium current traces on rat cardiac myocytes in the absence or presence of 1 μM JZTX-II. (D) Represent the typical TTX-R sodium currents traces on rat DRG neurons in the absence or presence of 10 μM JZTX-II. (E) 10 μM JZTX-II had no significant effect on TTX-S sodium channels in rat hippocampal neurons. (F) The concentration-dependent inhibition of sodium channels fast inactivation by JZTX-II. Every point (mean ± S.E.) comes from 3 to 6 separated experimental cells. These data points were fitted according to the Boltzmann equation.

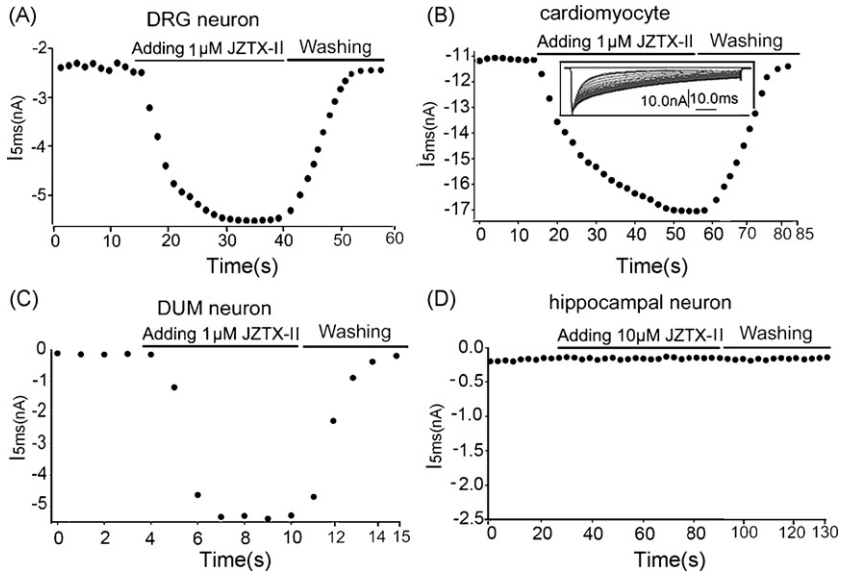

Fig. 4 – Time–effect curves of JZTX-II on sodium currents. (A) 1 μM JZTX-II could inhibit TTX-S sodium channels inactivation on rat DRG neurons and reached the maximal degree in 15 s. (B) 1 μM JZTX-II could inhibit the TTX-R sodium channels inactivation on the cardiomyocytes and reached the maximal degree in 30 s. (C) 1 μM JZTX-II could inhibit the TTX-S sodium channels inactivation rapidly on cockroach DUM neuron and reached the maximal degree in 3 s. (D) 10 μM JZTX-II had no significant inhibition on TTX-S sodium channels of hippocampal neurons. The current values come form the I_{5ms} of the current traces.

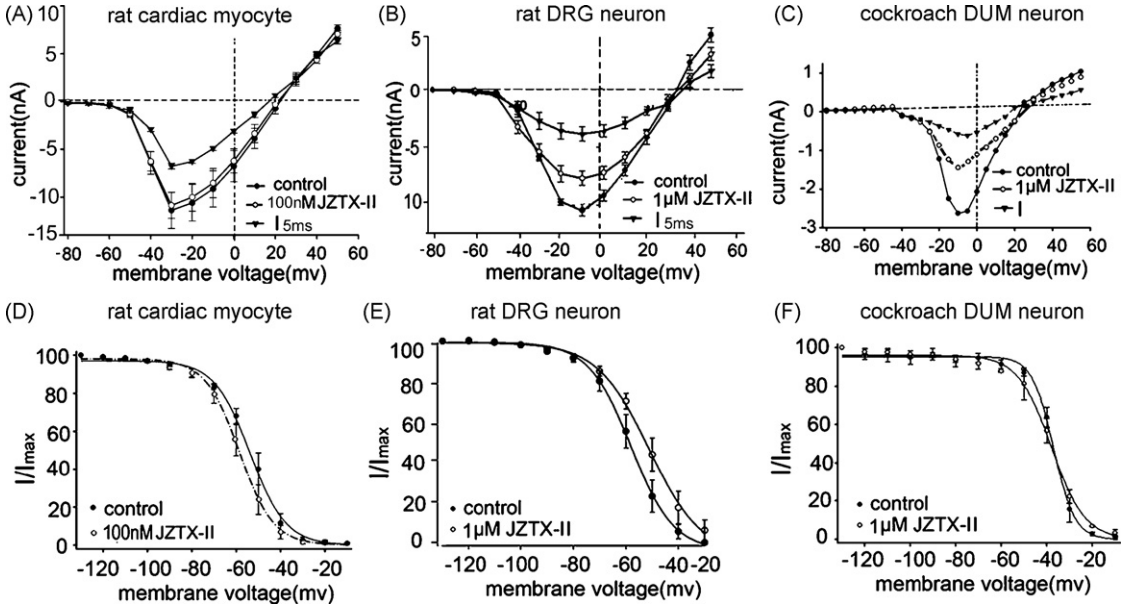

Fig. 5 – Effects of JZTX-II on current–voltage relationship and the steady-state inactivation of sodium channels. TTX-S currents on rat DRG neurons were induced to various test potentials (−80 mV to 50 mV) by 50 ms depolarizing from a holding potential of −80 mV with 10 mV increment. The current–voltage curves showed the current changes before (control) and after adding JZTX-II at different concentrations on rat cardiac myocytes (A), DRG neurons (B) and cockroach DUM neurons (C), respectively. I_{5ms} was shown as the current inactivated at 5 ms. The steady-state inactivation currents were induced by a 50 ms depolarizing potential of −10 mV from different prepulse potentials for 1 s which ranged from −130 mV to −10 mV or −20 mV with a 10 mV increment. The data dots shown as the ratio of I_{test} to I_{max} were fitted according to the Boltzmann equation: $I_{test}/I_{max} = 1/(1 + \exp((V - V_{1/2})/K))$, where V was the prepulse potential, $V_{1/2}$ values were shifted only by 4.8 mV (−53.7 ± 0.77 mV to −58.5 ± 0.83 mV) on cardiac myocytes sodium currents to hyperpolarization (D), by 5.9 mV (−59.0 ± 0.96 mV to −53.1 ± 0.93 mV) to depolarization (E) on rat DRG neurons and almost no shift (−38.0 ± 0.58 mV to −37.1 ± 0.44 mV) was observed on cockroach DUM neurons (F).

control conditions. After holding at a resting potential of −80 mV, the TTX-S sodium currents on rat DRG neurons and TTX-R sodium currents were initially elicited at −40 mV and reversed at about +30 mV while sodium currents elicited and reversed at −40 and +20 mV on insect neuron. 1 μM JZTX-II had no effect on the activating voltages and reversal potentials of various VGSCs (Fig. 5A–C, $n = 5$), although the slowing of channel inactivation was detected at the depolarized potentials ranging from −30 mV to +30 mV. The effect of JZTX-II on the steady-state inactivation of TTX-S VGSCs was determined by using a standard two-pulse protocol as detailed in Fig. 5. Sodium currents recorded following the prepulse potential from −130 mV to −10 mV were normalized to the maximal current and plotted against the conditioning prepulse potentials. In the presence of 1 μM JZTX-II, the half-maximal inactivation potential was shifted only from −54.2 mV to −58.0 mV in rat cardiac myocytes (Fig. 5D), from −59.0 mV to −53.1 mV in DRG neurons (Fig. 5E) and only from −37.1 mV to −38.3 mV in cockroach DUM neurons (Fig. 5F), respectively, thus suggesting that the toxin had no significant action on the steady-state inactivation of mammal and insect neuronal sodium channels.

3.5. *Effect of JZTX-II on calcium and potassium channels of Rat DRG neurons*

It is widely accepted that rat DRG neurons exhibit two categories of Cav channels: low-voltage activated (LVA) channels (T type) and high-voltage activated (HVA) channels (N, L, P/Q and R type), which can be discriminated by their voltage dependence and kinetics. The results showed that no significant inhibition was observed on both kinds of calcium currents when 10 μM JZTX-II was applied on DRG neurons (Fig. 6A and B). 10 μM JZTX-II had no significant effect on delayed-rectifier potassium currents (Fig. 6C) and the transient outward potassium currents (Fig. 6D) on DRG neurons, also.

4. Discussion

Spider venoms contain many neurotoxins with distinct biological activities. Most of them are toxic to vertebrates and insects, leading to an invaluable resource for exploration of medical drugs, safe insecticides and novel ligands for discovering the relationships between structure and function of ion channels [8]. In this work, we have characterized a novel VGSC inhibitor, jingzhaotoxin-II, from the Chinese tarantula *C. jingzhao* venom [30]. JZTX-II at high dose had no significant effect to calcium and potassium channel on DRG neurons (Fig. 6). The toxin was found to contain 32 residues including six cysteine residues (Fig. 2A). Conforming exactly to the ICK definition, the toxin is inferred to contain conserved disulfide connectivity (I–IV, II–V, and III–VI, Fig. 2A).

The cDNA sequence of JZTX-II encodes a precursor consisting of a signal peptide, an intervening propeptide, and a mature peptide, suggesting that post-translational cleavage is needed for producing mature JZTX-II. A Genebank database search indicated that the cDNA structure of JZTX-II is similar to most other spider cDNA sequences. In spite of coming from the same venom, JZTX-I, JZTX-II, JZTX-III and JZTX-XI have very different motif in cDNA. The JZTX-III precursor has an uncommon signal site (-X-Ser-) and JZTX-II contains a site common (-X-Arg-) to most animal toxin precursors such as JZTX-I and JZTX-XI [13,14,24] and the propeptide region length (10 residues) in JZTX-II is much shorter than that (29 residues) of JZTX-XI similar to that of JZTX-I (8 residues) and much longer than that of JZTX-III (5 residues) [12,13,16]. Generally, the similarities of the pre-propeptide sequences are important criteria for defining the subfamilies of naturally occurring toxins. JZTX-II pre-propeptide shows 80.9% and 87.5% sequence identity with JZTX-I pre-propeptide in signal peptide and intervening propeptide, while sharing only 63.6% and 20% with JZTX-III pre-propeptide and the difference is even more with JZTX-XI, inferring that JZTX-II and JZTX-I might belong to the same sub-family different from JZTX-III and JZTX-XI belong to.

The phylogeny of spider sodium channel toxins based on their amino acid sequences in Fig. 7 indicated that the toxins are divergent in two evolutionary routes, the toxins from the family *Theraphosidae* and *Hexathelidae* which has a large body size are clustered in the first group, whereas toxins from the family *Agelenopsis* which has a small body size are clustered into the second branch, suggesting that they derive from different ancestor. From the phylogeny, we deduce that JZTXs

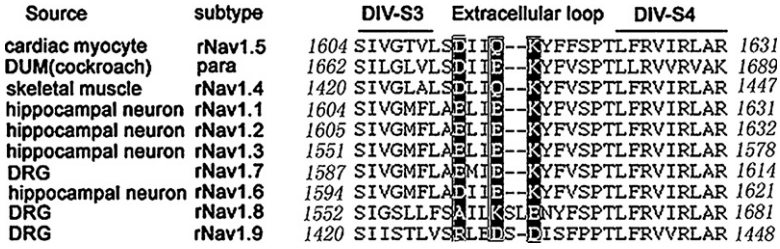

Fig. 6 – Effects of JZTX-II to calcium channels and potassium channels. Ca^{2+} had been substituted by Ba^{2+}. (A) High-voltage activated Ca^{2+} currents had been induced by 100 ms depolarization step to 0 mV from a holding potential of −40 mV. 10 μM JZTX-II could not inhibit HVA Ca^{2+} currents ($n = 5$). (B) Low-voltage activated Ca^{2+} currents were elicited by 100 ms depolarization step to −50 mV from a holding potential of −90 mV. 10 μM JZTX-II had no effect to T type calcium currents. (C) Delayed-rectifier potassium currents had been elicited by 100 ms depolarization step to 30 mV from a holding potential of −80 mV. 10 μM JZTX-II had no significant effect on the delayed-rectifier potassium currents ($n = 5$). (D) Transient outward potassium currents had been induced by 300 ms depolarization step to 30 mV from a holding potential of −80 mV. 10 μM JZTX-II had no effect on the transient outward potassium currents of DRG neurons ($n = 5$).

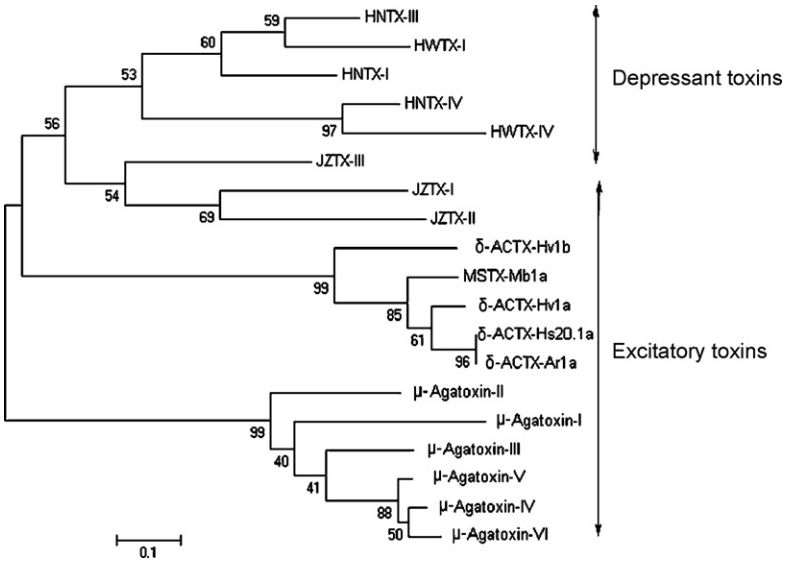

Fig. 7 – Analysis of amino acid sequences of receptor site 3 on different rat sodium channel subtypes. The sequences of various sodium channel subtypes are from NCBI databank. The number represents the superimposed position of amino acid of various sodium channels. The putative crucial residues between toxins and sodium channels are shaded in black.

lie between the depressant toxins, HNTXs, HWTXs and the excitatory toxins δ-ACTXs, μ-agatoxins not only in sequence but also in function. HWTXs and HNTXs are depressant spider toxins through the peak current similar to TTX [31]. δ-Atracotoxins induce spontaneous repetitive firing and prolongation of action potentials resulting in neurotransmitter release from somatic and autonomic nerve endings [8]. The μ-agatoxins cause increased spontaneous release of neurotransmitter from pre-synaptic terminals and repetitive action potentials in motor neurons [32]. JZTXs might give some important insight into toxin evolution. Intriguingly, JZTXs have much more diversity of function than the other three kinds of spider toxins in functions.

Animal toxins targeting sodium channels can be classified into two groups according to their distinct pharmacological properties: blockers (e.g. tetrodotoxin and μ-conotoxin) and modulators (e.g. δ-atracotoxin, batrachotoxin, α- and β-scorpion toxins, and sea anemone toxins) [33]. JZTX-II preferentially inhibits cardiac sodium channel inactivation ($IC_{50} = 0.26 \pm 0.09$ μM) and potential activities to TTX-S VGSCs in rat DRG neurons and weak effect in cockroach DUM neurons without affecting TTX-S VGSCs in rat hippocampal neurons and TTX-R VGSCs in rat DRG neurons. The data showed that JZTX-II exhibited a similar manner to δ-atracotoxins, scorpion α-toxins and sea anemones [4,13,8,34], indicating its role as a modulator of VGSCs. Its potential modulating site is reasonably assumed to be receptor site 3. Among all known toxins, JZTX-II shows the most functional consistencies with BgII and BgIII from sea anemone *Bunodosoma granulifera*, which inhibits sodium channels on rat DRG neurons, cardiac muscle and insect neurons [33,34]. To the best of our knowledge, there are no related reports about the effect of BgII and BgIII in hippocampal neurons. JZTX-II is a unique toxin reported to date produce a specific effect on cardiac myocytes and TTX-S VGSCs in DRG neurons rather than TTX-R VGSCs in DRG neurons (subtypes rNav1.8, rNav1.9) and TTX-S VGSCs in hippocampal neurons. Given the high specificity of JZTX-II to various sodium channel subtypes, JZTX-II might be a useful probe for discriminating rat cardiac TTX-R VGSC (subtype rNav1.5) from the other two TTX-R VGSCs (rNav1.8, rNav1.9), and might be used to distinguish TTX-S VGSCs in DRG neurons from the other TTX-S VGSCs in central neurons.

Rogers et al. found that Glu^{1613}, Glu^{1616}, Lys^{1617} and six uncharged residues of the IVS3–S4 loop in type rIIa sodium channel that significantly affected LqTx and/or ATX II affinity and constituted an important component of neurotoxin receptor site 3 [35]. Moreover, chimeric Na^+ channels in which amino acid residues at the extracellular end of segment IVS3 of the a subunit of cardiac Na^+ channels were substituted into the type IIa channel sequence had reduced affinity for α-scorpion toxin characteristic of cardiac Na^+ channels. Thus, JZTX-II had opposite affinity. Based on the sequences of various sodium channel subtypes in Fig. 8 and the properties of toxins altering channel gating, JZTX-II might structurally interact with receptor site 3 and its two charged residues (Lys^{13} and Glu^{12}, Fig. 2A) might provide key residues for binding the residues Asp^{1612} and Lys^{1616} in rNav1.5 but not Glu^{1613}, Glu^{1616}, Lys^{1617} in rNav1.2 and other subtypes in brain. Since the two residues are highly conserved in skeletal muscle sodium channel (rNav1.4) and rNav1.5 in Fig. 6, Nav1.4 might be also sensitive to JZTX-II. Sodium channel isoforms preferentially express in specific tissues. Felts and co-workers demonstrated that rNav1.1, rNav1.2, rNav1.3 and rNav1.6 are expressed predominantly in rat embryonic hippocampus neurons [24,36]. Intriguingly, our findings indicated that JZTX-II had no effect on sodium channel subtypes from embryonic hippocampus neurons. We concluded JZTX-II had high affinity to sodium channel subtype on cardiac myocytes but lower affinity to subtypes on DRG neurons and almost no affinity to that on brain. The different option between JZTX-II and LqTx might hint the different interactions between the sodium

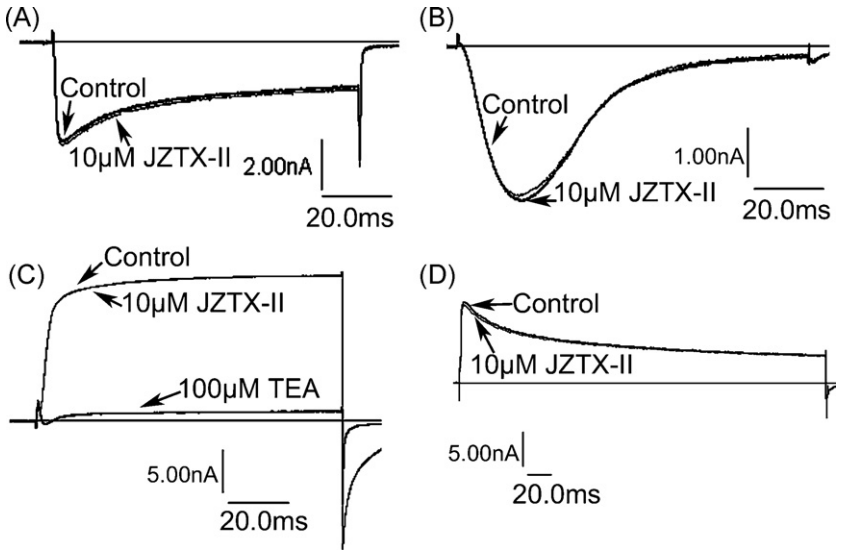

Fig. 8 – Unrooted phylogenetic tree of spider sodium channel toxins. The numbers on the branches were the bootstrap percentages supporting a given partition. The main characteristic functions of these spider toxins are shown on the right.

channel subtypes and toxins. JZTX-II represents a new interaction model.

Sequence alignment in Fig. 2A indicates that JZTX-II shows limited sequence identity with other sodium channel toxins. HNTX-IV is a potent blocker of neuronal TTX-S VGSCs on rat DRG neurons with an IC_{50} value of 44.6 nM [37]. Substitutions of Lys^{27} or Arg^{29} with Ala reduce the effect of HNTX-IV on TTX-S VGSC on DRG neurons by over 10-fold. The two positively charged residues are also conserved in HWTX-IV. Both of them are assumed not to interact with receptor site 3 on sodium channels. However, the residue Lys^{27} in HWTX-IV and HNTX-IV is replaced by Ala^{24} in JZTX-II, but the other basic residue is conserved among the three toxins (Fig. 2A). We do not know whether Lys^{26} is crucial for JZTX-II altering channel gating or the weak reduction of peak current. It is interesting that δ-conotoxin EVIA inhibit the inactivation of sodium channels from mammal ion neurons (rNav1.2, rNav1.3 and rNav1.6) but has no effect on rat skeletal muscle (rNav1.4) and human cardiac muscle (hNav1.5) sodium channels [38,39], which have a very different selectivity from JZTX-II.

In contrast to pore-blocking toxins, the kinetics of onset of inhibition by JZTX-II is slow, similar to JZTX-XI and other gating modifier toxins [16]. The slow inhibition kinetics of the toxin may be related to the rate of membrane partitioning or the efficiency of the toxin channel binding step or by a combination of both effects according to previous work by Seok-Yong Lee et al. JZTX-III and JZTX-XI are two tarantula toxins taken from *C. jingzhao* and found to target cardiac sodium channels and Kv2.1 channel. Their three-dimensional structures have been recently resolved using NMR technique [14,16]. They adopt a common ICK motif composed of two or three β-strands. A structural comparison of JZTX-III and JZTX-XI with those of other ICK motif peptides (e.g. Hanatoxin1 and SGTx1) shows that they all adopt a conserved surface profile, with a hydrophobic patch (Met^5, Phe^6, and Trp^{30} in JZTX-XI) surrounded by charged residues (Arg^3, Lys^{22}, and Asp^{31} in JZTX-XI) which might be the crucial site for voltage-gating ion channel inhibition [16]. The sequence alignment in Fig. 2A indicates that JZTX-II shows limited sequence identities with the two toxins. However, interestingly, several hydrophobic residues (Met^5, Trp^6, and Trp^{30}) in JZTX-II are conserved at the corresponding positions in other sodium channel toxins. The toxin, JZTX-II, isolated from the same spider venom, was deduced to have Janus-like bioactive surface, a hydrophobic patch (Met^5, Trp^6, Trp^{30}) and a charged boundary (Glu^{12}, Lys^{13}, Lys^{26}).

Although the usefulness of these natural toxins as substitutes for the currently available therapeutics is limited, they clearly display high sodium channel affinity, resulting in potent cardiotonic activity. Therefore, an understanding of the molecular basis for their interaction with the sodium channel will provide valuable information for the design of novel synthetic drugs having enhanced positive inotropic activity.

Acknowledgements

We greatly appreciate Professor Xian-Chun Wang, Ying Wang for revising the manuscript. The work was supported by the National Nature Science Foundation of China under Contract Nos. 30430170, 30500146, 30370260, 30670640, 30700127, ''973 program'': 2006CB708508, National ''863'' specific topic of 2006AA02Z141 and scientific research fund of Hunan Normal University: 050633.

REFERENCES

[1] Nassar MA, Stirling LC, Forlani G, Baker MD, Matthews EA, Dickenson AH, et al. Nociceptor-specific gene deletion reveals a major role for Nav1,7 (PN1) in acute and inflammatory pain. Proc Natl Acad Sci U S A 2004;101: 12706–11.

[2] Catterall WA. Cellular and molecular biology of voltage-gated sodium channels. Physiol Rev 1992;72:S15–48.
[3] Waxman SG. Acquired channelopathies in nerve injury and MS. Neurology 2001;56:1621–7.
[4] Goudet C, Ferrer T, Galan L, Artiles A, Batista CF, Possani LD, et al. Characterization of two *Bunodosoma granulifera* toxins active on cardiac sodium channels. Br J Pharmacol 2001;134:1195–206.
[5] Leipold E, Lu S, Gordon D, Hansel A, Heinemann SH. Combinatorial interaction of scorpion toxins Lqh-2, Lqh-3, and LqhalphaIT with sodium channel receptor sites-3. Mol Pharmacol 2004;65:685–91.
[6] Gordon D, Gurevitz M. The selectivity of scorpion alpha-toxins for sodium channel subtypes is determined by subtle variations at the interacting surface. Toxicon 2003;41:125–8.
[7] Oliveira JS, Redaelli E, Zaharenko AJ, Cassulini RR, Konno K, Pimenta DC, et al. Binding specificity of sea anemone toxins to Nav 1,1-1.6 sodium channels: unexpected contributions from differences in the IV/S3–S4 outer loop. J Biol Chem 2004;279:33323–35.
[8] Nicholson GM, Little MJ, Birinyi-Strachan LC. Structure and function of delta-atracotoxins: lethal neurotoxins targeting the voltage-gated sodium channel. Toxicon 2004;43:587–99.
[9] Grolleau F, Stankiewicz M, Birinyi-Strachan L, Wang XH, Nicholson GM, Pelhate M, et al. Electrophysiological analysis of the neurotoxic action of a funnel-web spider toxin, delta-atracotoxin-HV1a, on insect voltage-gated Na^+ channels. J Exp Biol 2001;204:711–21.
[10] Leipold E, Hansel A, Borges A, Heinemann SH. Subtype specificity of scorpion beta-toxin Tz1 interaction with voltage-gated sodium channels is determined by the pore loop of domain 3. Mol Pharmacol 2006;70:340–7.
[11] Smith JJ, Cummins TR, Alphy S, Blumenthal KM. Molecular interactions of the gating modifier toxin ProTx-II with Nav1,5: implied existence of a novel toxin binding site coupled to activation. J Biol Chem 2007;282:12687–9.
[12] Xiao Y, Tang J, Hu W, Xie J, Maertens C, Tytgat J, et al. Jingzhaotoxin-I, a novel spider neurotoxin preferentially inhibiting cardiac sodium channel inactivation. J Biol Chem 2005;280:12069–76.
[13] Xiao Y, Tang J, Yang Y, Wang M, Hu W, Xie J, et al. Jingzhaotoxin-III, a novel spider toxin inhibiting activation of voltage-gated sodium channel in rat cardiac myocytes. J Biol Chem 2004;279:26220–6.
[14] Liao Z, Yuan C, Peng K, Xiao Y, Liang S. Solution structure of Jingzhaotoxin-III, a peptide toxin inhibiting both Nav1,5 and Kv2.1 channels. Toxicon 2007;50:135–43.
[15] Zeng X, Deng M, Lin Y, Yuan C, Pi J, Liang S. Isolation and characterization of Jingzhaotoxin-V, a novel neurotoxin from the venom of the spider *Chilobrachys jingzhao*. Toxicon 2007;49:388–99.
[16] Liao Z, Yuan C, Deng M, Li J, Chen J, Yang Y, et al. Solution structure and functional characterization of jingzhaotoxin-XI: a novel gating modifier of both potassium and sodium channels. Biochemistry 2006;45:15591–600.
[17] Yuan C, Liao Z, Zeng X, Dai L, Kuang F, Liang S. Jingzhaotoxin-XII a gating modifier specific for Kv4,1 channels. Toxicon 2007;50:507–17.
[18] Alewood D, Birinyi-Strachan LC, Pallaghy PK, Norton RS, Nicholson GM, Alewood PF. Synthesis and characterization of delta-atracotoxin-Ar1a, the lethal neurotoxin from venom of the Sydney funnel-web spider (*Atrax robustus*). Biochemistry 2003;42:12933–40.
[19] Liang SP, Zhang DY, Pan X, Chen Q, Zhou PA. Properties and amino acid sequence of huwentoxin-I, a neurotoxin purified from the venom of the Chinese bird spider *Selenocosmia huwena*. Toxicon 1993;3:969–78.
[20] Macianskiene R, Bito V, Raeymaekers L, Brandts B, Sipido KR, Mubagwa K. Action potential changes associated with a slowed inactivation of cardiac voltage-gated sodium channels by KB130015. Br J Pharmacol 2003;139:1469–79.
[21] Wicher D, Walther C, Penzlin H. Neurohormone D induces ionic current changes in cockroach central neurons. J Comp Physiol 1994;174:507–15.
[22] Wicher D, Penzlin H. Ca^{2+} currents in central insect neurons: electrophysiological and pharmacological properties. J Neurophysiol 1997;77:186–99.
[23] Chen P, Li X, Sun Y, Liu Z, Cao R, He Q, et al. Proteomic analysis of rat hippocampal plasma membrane: characterization of potential neuronal-specific plasma membrane proteins. J Neurochem 2006;98:1126–40.
[24] Alami M, Vacher H, Bosmans F, Devaux C, Rosso JP, Bougis PE, et al. Characterization of Amm VIII from *Androctonus mauretanicus mauretanicus*: a new scorpion toxin that discriminates between neuronal and skeletal sodium channels. Biochem J 2003;375:551–60.
[25] Fletcher JI, Chapman BE, Mackay JP, Howden ME, King GF. The structure of versutoxin (delta-atracotoxin-Hv1) provides insights into the binding of site 3 neurotoxins to the voltage-gated sodium channel. Structure 1997;5:1525–35.
[26] Kozlov S, Grishin E. Classification of spider neurotoxins using structural motifs by primary structure features, single residue distribution analysis and pattern analysis techniques. Toxicon 2005;46:672–86.
[27] Caffrey JM, Eng DL, Black JA, Waxman SG, Kocsis JD. Three types of sodium channels in adult rat dorsal root ganglion neurons. Brain Res 1992;592:283–97.
[28] Mechaly I, Scamps F, Chabbert C, Sans A, Valmier J. Molecular diversity of voltage-gated sodium channel alpha subunits expressed in neuronal and non-neuronal excitable cells. Neuroscience 2005;130:389–96.
[29] Kerr NC, Holmes FE, Wynick D. Novel isoforms of the sodium channels Nav1,8 and Nav1. 5 are produced by a conserved mechanism in mouse and rat. J Biol Chem 2004;279:24826–33.
[30] Zhu M, Song D, Li T. J Baoding Teach Coll (Chinese) 2001;14:1–6.
[31] Li D, Xiao Y, Hu W, Xie J, Bosmans F, Tytgat J, et al. Function and solution structure of hainantoxin-I, a novel insect sodium channel inhibitor from the Chinese bird spider *Selenocosmia hainana*. FEBS Lett 2003;555:616–22.
[32] Adams ME. Agatoxins: ion channel specific toxins from the American funnel web spider *Agelenopsis aperta*. Toxicon 2004;43:509–25.
[33] Salceda E, Garateix A, Soto E. The sea anemone toxins BgII and BgIII prolong the inactivation time course of the tetrodotoxin-sensitive sodium current in rat dorsal root ganglion neurons. J Pharmacol Exp Ther 2002;303:1067–74.
[34] Bosmans F, Aneiros A, Tytgat J. The sea anemone *Bunodosoma granulifera* contains surprisingly efficacious and potent insect-selective toxins. FEBS Lett 2002;532: 131–4.
[35] Rogers JC, Qu Y, Tanada TN, Scheuer T, Catterall WA. Molecular determinants of high affinity binding of alpha-scorpion toxin and sea anemone toxin in the S3–S4 extracellular loop in domain IV of the Na^+ channel alpha subunit. J Biol Chem 1996;271:15950–62.
[36] Mechalv I, Scamps F, Chabbert C, Sans A, Valmier J. Molecular diversity of voltage-gated sodium channel alpha subunits expressed in neuronal and non-neuronal excitable cells. Neuroscience 2005;130:389–96.
[37] Li D, XiaoY, Xu X, Xiong X, Lu S, Liu Z, et al. Structure–activity relationships of hainantoxin-IV and structure determination of active and inactive sodium channel blockers. J Biol Chem 2004;279:37734–40.

[38] Barbier J, Lamthanh H, Le Gall F, Favreau P, Benoit E, Chen H, et al. A delta-conotoxin from *Conus ermineus* venom inhibits inactivation in vertebrate neuronal Na^+ channels but not in skeletal and cardiac muscles. J Biol Chem 2004;279:4680–5.

[39] Volpon L, Lamthanh H, Barbier J, Gilles N, Molgo J, Menez A, et al. NMR solution structures of delta-conotoxin EVIA from *Conus ermineus* that selectively acts on vertebrate neuronal Na^+ channels. J Biol Chem 2004;279:21356–6.